

pubs.acs.org/est Article

# Removal of CrO<sub>4</sub><sup>2-</sup>, a Nonradioactive Surrogate of <sup>99</sup>TcO<sub>4</sub><sup>-</sup>, Using LDH–Mo<sub>3</sub>S<sub>13</sub> Nanosheets

Ahmet Celik, Dien Li, Michael A. Quintero, Kathryn M. L. Taylor-Pashow, Xianchun Zhu, Mohsen Shakouri, Subrata Chandra Roy, Mercouri G. Kanatzidis, Zikri Arslan, Alicia Blanton, Jing Nie, Shulan Ma, Fengxiang X. Han, and Saiful M. Islam\*



Cite This: Environ. Sci. Technol. 2022, 56, 8590-8598



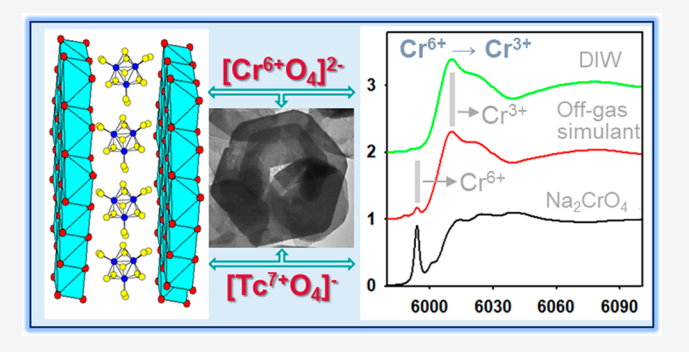
**ACCESS** 

Metrics & More

Article Recommendations

Supporting Information

ABSTRACT: Removal of chromate  $(\text{CrO}_4^{\,2^-})$  and pertechnetate  $(\text{TcO}_4^{\,-})$  from the Hanford Low Activity Waste (LAW) is beneficial as it impacts the cost, life cycle, operational complexity of the Waste Treatment and Immobilization Plant (WTP), and integrity of vitrified glass for nuclear waste disposal. Here, we report the application of  $[\text{Mo}^{\text{IV}}_3\text{S}_{13}]^{2^-}$  intercalated layer double hydroxides (LDH–Mo<sub>3</sub>S<sub>13</sub>) for the removal of  $\text{CrO}_4^{\,2^-}$  as a surrogate for  $\text{TcO}_4^{\,-}$ , from ppm to ppb levels from water and a simulated LAW off-gas condensate of Hanford's WTP. LDH–Mo<sub>3</sub>S<sub>13</sub> removes  $\text{CrO}_4^{\,2^-}$  from the LAW condensate stream, having a pH of 7.5, from ppm (~9.086 × 10<sup>4</sup> ppb of  $\text{Cr}^{6^+}$ ) to below 1 ppb levels with distribution constant  $(K_d)$  values of up to ~10<sup>7</sup> mL/g.



Analysis of postadsorbed solids indicates that  $CrO_4^{2-}$  removal mainly proceeds by reduction of  $Cr^{6+}$  to  $Cr^{3+}$ . This study sets the first example of a metal sulfide intercalated LDH for the removal of  $CrO_4^{2-}$ , as relevant to  $TcO_4^{-}$ , from the simulated off-gas condensate streams of Hanford's LAW melter which contains highly concentrated competitive anions, namely  $F^-$ ,  $Cl^-$ ,  $CO_3^{2-}$ ,  $NO_3^{-}$ ,  $BO_3^{3-}$ ,  $NO_2^{-}$ ,  $SO_4^{2-}$ , and  $B_4O_7^{2-}$ . LDH $-Mo_3S_{13}$ 's remarkable removal efficiency makes it a promising sorbent to remediate  $CrO_4^{2-}/TcO_4^{-}$  from surface water and an off-gas condensate of nuclear waste.

KEYWORDS: nuclear waste, pertechnetate, chromate, low activity waste, off-gas condensate stream, Hanford's radioactive waste

#### ■ INTRODUCTION

The Hanford Waste Treatment and Immobilization Plant (WTP), the DOE's largest nuclear waste treatment plant, is designed to process, treat, and immobilize much of the radioactive legacy wastes.<sup>1–4</sup> The current plan of the Hanford Waste Treatment and Immobilization Plant (WTP) is to separate the tank wastes into high-level waste (HLW) and lowactivity waste (LAW) and permanently immobilize the radioisotopes into separately vitrified waste forms.5 LAW constitutes a larger fraction of the waste by volume, and it consists of high ionic-strength solutions that contain Na<sup>+</sup>, K<sup>+</sup>,  $Al(OH)_4^-$ ,  $Cl^-$ ,  $F^-$ ,  $NO_2^-$ ,  $NO_3^-$ ,  $OH^-$ ,  $CO_3^{2-}$ , organics, other minor ions of Cr, Ni, Cd, and Pb, and radionuclides.<sup>6</sup> Technetium-99 (<sup>99</sup>Tc) is a β-emitting long living,  $t_{1/2} \sim 2.13 \times$  $10^5$  years, radionuclide which mostly remains in LAW as  ${\rm TcO_4}^{-4,7-10}$  Immobilization of  ${\rm TcO_4}^-$  at the WTP becomes challenging because of its high solubility, complex redox chemistry, and volatility at the vitrification temperature. 4,7-10 The treatment and vitrification of LAW at the Hanford WTP will generate an aqueous LAW off-gas condensate which is planned to be repeatedly reprocessed and passed through the glass melter until nearly complete immobilization of technetium. 4,8,11 This procedure results in the increase of the WTP operational time, waste volume, and vitrification cost. Importantly, this process could be limited for extremely low concentrations, namely  $\leq 5$  ppb. Also, the off-gas condensate contains halides and chromates which have a detrimental effect on the glass formulation during the vitrication. <sup>12–14</sup> Therefore, it is important to develop materials, methods, and technologies to redirect the technetium immobilization from LAW.

With a reduction potential of -0.22 V (for the  $S^2-/SO_4^{2-}$  couple), sulfides are capable of reducing the highly soluble  $TcO_4^-$  ( $TcO_4^-/Tc^{4+}$  is  $E^\circ \sim +0.74$  V) and  $CrO_4^{2-}$  ( $CrO_4^{2-}/Cr^{3+}$  is  $E^\circ \sim +1.23$  V) ions to insoluble Tc(IV) and Cr(III) species.  $^{6,15-21}$  Because of the known chemistry of sulfides and other reductants for the reductive precipitation of highly redoxactive  $Tc^{7+}$  and  $Cr^{6+}$ , we introduced  $(Cr^{6+}O_4)^{2-}$  as a nonradioactive surrogate for a reductive precipitation driven

Received: January 15, 2022
Revised: May 13, 2022
Accepted: May 16, 2022
Published: June 1, 2022





separation.  $^{1,9,22,23}$  In addition to being a suitable surrogate for  $TcO_4^-$ ,  $CrO_4^{2-}$  itself is highly toxic<sup>24</sup> and also persists within the radioactive waste of the Hanford nuclear waste streams.  $^{25-27}$  Because of the leakage in the Hanford underground tanks, chromate has been dispersing in the environment along with various radionuclides.  $^{28-30}$  Moreover, during the vitrification process of the LAW,  $CrO_4^{2-}$  is transformed into crystalline spinel which in turn jeopardizes the integrity of the glass waste form.  $^{13,31}$  Therefore, in addition to pertechnetate, it is crucial to remediate chromate from water and legacy nuclear wastes.

Numerous metal sulfides, such as pyrrhotite  $(Fe_{1-x}S)$  and pyrite  $(FeS_2)$ ,  $^{32,33}$  chalcocite  $(Cu_2S)$ ,  $^{29,30}$  and stibnite  $(Sb_2S_3)$ ,  $^{34}$  and layered metal sulfides are known to immobilize  $TcO_4^-$  by reductive precipitation.  $^{15,16}$  Layered double hydroxides (LDHs) are anionic clays which can also remove  $TcO_4^-/CrO_4^{2-}$  but with ion-exchange and surface sorption mechanisms.  $^{8,15,24,35}$  Considering the efficiency of LDH and metal sulfides for  $TcO_4^-/CrO_4^{2-}$  remediation, we hypothesized that a hybrid structure of metal sulfide intercalated LDH will boost the removal of pertechnetate from water and legacy nuclear waste. Altogether, it becomes important to investigate LDH-metal sulfide based materials, evaluate the remediation of  $TcO_4^-$ , and delineate the sorption mechanisms involved in this process.

Herein, we report a modified synthesis method for LDH– $\mathrm{Mo_3}\mathrm{S_{1}}^{36}$  to achieve nanosheets and the investigation of  $\mathrm{CrO_4}^{2-}$ , which also acts as a  $\mathrm{TcO_4}^-$  surrogate, sorption from naturally contaminated surface water, and a simulated off-gas condensate of the LAW melter. We show that LDH– $\mathrm{Mo_3}\mathrm{S_{13}}$  exhibits ultrahigh efficient sorption of  $\mathrm{CrO_4}^{2-}$  from water and an off-gas condensate from ppm to ppb levels (<1 ppb) with  $K_{\rm d}$  values of up to  $\sim 10^7$  mL/g. For LDH– $\mathrm{Mo_3}\mathrm{S_{13}}$ , we show that reductive precipitation is the dominant mechanism; however, ion-exchange and/or surface sorption can provide parallel paths for the sequestration of  $\mathrm{CrO_4}^{2-}$ . These integrated multimode sorption processes make LDH– $\mathrm{Mo_3}\mathrm{S_{13}}$  a promising sorbent of  $\mathrm{CrO_4}^{2-}/\mathrm{TcO_4}^-$  from polluted water and nuclear waste.

## EXPERIMENTAL SECTION

Material Synthesis and Chromate Uptake Study. MgAl-CO<sub>3</sub> (LDH-CO<sub>3</sub>), MgAl-NO<sub>3</sub> (LDH-NO<sub>3</sub>), and  $(NH_4)_2Mo_3S_{13}\cdot H_2O$  were synthesized as previously described.  $^{37-40}$  LDH $-Mo_3S_{13}$  nanosheets were synthesized with a two-step method: first, exfoliation of LDH nanosheets of the LDH-NO<sub>3</sub> and then the settlement of positively charged LDH sheets in the presence of dissolved Mo<sub>3</sub>S<sub>13</sub><sup>2</sup> anions. More specifically, 200 mg of LDH-NO3 was added to 20 mL of formamide and stirred for 24 h to exfoliate the positively charged LDH nanosheets. Afterward, a solution of 200 mg of (NH<sub>4</sub>)<sub>2</sub>Mo<sub>3</sub>S<sub>13</sub>·H<sub>2</sub>O in 2 mL of formamide was slowly added to the exfoliated LDH solution and stirred for 30 min. Later, the solution was left at ambient conditions for 2 h, filtered, then washed with water and acetone, and subsequently dried at ambient conditions to give a brown solid of LDH-Mo<sub>3</sub>S<sub>13</sub>. Thus, this process of synthesis differs from the previously reported synthesis of LDH-Mo<sub>3</sub>S<sub>13</sub>.<sup>36</sup>

Chromate Uptake Study. LDH-Mo<sub>3</sub>S<sub>13</sub> was added to the CrO<sub>4</sub><sup>2-</sup> spiked solutions at different concentrations, stirred for different periods of time, and centrifuged to separate the supernatant solution from the solids. For the Hanford's LAW off-gas condensate simulated streams, the sorption study was

conducted by the batch method by spiking the simulant with 9.086  $\times$   $10^4$  ppb of  $Cr^{6+}$  as  $CrO_4^{\,2-}$  ( $CrO_4^{\,2-}$  equivalent concentrations  $\sim\!2.027\times10^5$  ppb), using variable loading of adsorbent, LDH–Mo $_3S_{13}$  (10 to 100 mg), and at variable time scales ( $\sim\!1$  h to 7 d), in 10 mL of simulated solutions, as described in Table S1.  $^{1.9}$  This study mostly focuses on the application of the LDH material for the remediation of  $CrO_4^{\,2-}/TcO_4^{\,-}$  from the high ionic strength simulated off-gas condensate streams of Hanford LAW waste at pH  $\sim$  7.5. Hence, the variation of the solution pH and ionic strengths was not monitored or controlled during the Cr uptake studies since these are not known for the real off-gas condensate streams as the WPT has not started this operation yet.

After the sorption experiments, the residual  ${\rm CrO_4}^{2-}$  concentrations in the supernatant were analyzed by inductively coupled plasma-mass spectrometry (ICP-MS). The adsorption capacity was determined from the difference in the concentrations of Cr before and after sorption.

The distribution coefficient  $(K_{\rm d})$  for the sorption of  ${\rm CrO_4}^{2-}$  was determined in accordance with the equations,  $K_{\rm d}=(V[(C_0-C_{\rm f})/C_{\rm f}])/m$ , where V is the solution volume (mL),  $C_0$  and  $C_{\rm f}$  are the initial and the final concentrations of  ${\rm CrO_4}^{2-}$  in ppm, and m is the mass of the solid sorbent (g). In this work, we used the  $K_{\rm d}$  values to compare the  ${\rm Cr}^{6+}$  removal performance with other adsorbents. The removal rate of  ${\rm CrO_4}^{2-}$  was computed using the equation of  $100\times(C_0-C_{\rm f})/C_0$ . The removal capacity,  $q_{\rm m}$  (mg/g), can be obtained from the following equation:  $10^{-3}\times(C_0-C_{\rm f})V/m$ . The adsorption experiments were carried out with V:m ratios of 100-1000 mL/g, at room temperature (RT) and at different time scales ranging from minutes to days.

The sorption kinetics of LDH– $Mo_3S_{13}$  was studied to determine the rate of removal of  $CrO_4^{2-}$  and to understand the sorption mechanism. In general, the adsorption rate is determined by two different rate equations, known as pseudo-first-order and pseudo-second-order mechanisms. Here, we used these mechanisms to analyze the adsorption phenomena of LDH– $Mo_3S_{13}$ . The comparison was then drawn between the experimental and calculated data in accordance with the rate equations, as follows<sup>42</sup>

Pseudo-first-order:

$$\ln(q_e - q_t) = \ln q_e - k_1 t \tag{1}$$

Pseudo-second-order:

$$\frac{\mathsf{t}}{q_{\mathsf{t}}} = \frac{1}{k_2 q_{\mathsf{e}}^2} + \frac{\mathsf{t}}{q_{\mathsf{e}}} \tag{2}$$

where  $q_{\rm e}$  (mg/g) is the amount of adsorbed element per unit mass of adsorbent at equilibrium, and  $q_{\rm t}$  (mg/g) is the adsorbed amount at time t, while  $k_1$  (min<sup>-1</sup>) and  $k_2$  (g/mg·min<sup>-1</sup>) are equilibrium rate constants of pseudo-first-order and pseudo-second-order adsorption interactions, respectively. The  $k_1$  value can be obtained by plotting  $\ln(q_{\rm e}-q_{\rm t})$  against t, and the  $k_2$  value can be obtained by plotting  $t/q_{\rm t}$  against t.

To understand the adsorbent and adsorbate interactions, we demonstrate the experimentally obtained adsorption data using the Langmuir isotherm model as given in eq 3. According to this model, the adsorbate moieties undergo monolayer type coverage on the surface of the adsorbent materials. It also predicts, once an adsorption site is occupied, no further adsorption can occur at the same site.<sup>44</sup> The Langmuir isotherm model for heterogeneous models is shown as eq 3

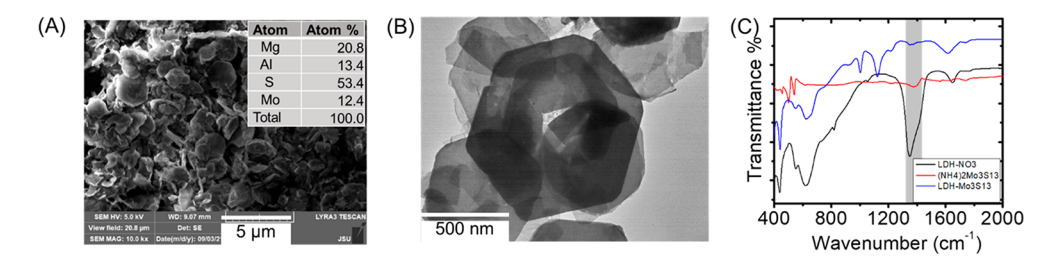


Figure 1. SEM image of the as-prepared LDH-Mo<sub>3</sub>S<sub>13</sub> (Insets show the average atomic abundance in percentage that was obtained by EDS.) (A), TEM image showing the ultrathin platelike morphology of the crystallites (B), and infrared spectrum showing the absence of NO<sub>3</sub><sup>-</sup> peaks from the LDH-Mo<sub>3</sub>S<sub>13</sub> indicating ion exchange of nitrate by the Mo<sub>3</sub>S<sub>13</sub> (C).

Langmuir isotherm: 
$$q = q_m \frac{bC_e}{1 + bC_e}$$
 (3)

where  $C_{\rm e}$  (mg/L) is the concentration at equilibrium, q (mg/g) is the equilibrium sorption capacity of the adsorbed  ${\rm CrO_4}^{2-}$ ,  $q_{\rm m}$  (mg/g) is the theoretical maximum sorption capacity, and b (L·mg<sup>-1</sup>) is the Langmuir constant which is related to the interaction energy of LDH–Mo<sub>3</sub>S<sub>13</sub> and  ${\rm CrO_4}^{2-}$ .

Characterization. Samples were analyzed by scanning electron microscopy (SEM), transmission electron microscopy (TEM), Energy Dispersive Spectroscopy (EDS), X-ray Powder Diffraction (XRD) and Infrared (FT-IR) Spectroscopy, Inductively Coupled Plasma-Mass Spectrometry (ICP-MS), and X-ray photoelectron spectroscopy (XPS) (see the Supporting Information for experimental details).

Synchrotron X-ray Absorption Spectroscopy. The solid samples after the chromate interactions in DIW and simulated solutions were dried at ambient conditions and analyzed by synchrotron X-ray absorption near edge structure (XANES) and extended X-ray absorption fine structure (EXAFS). S K-edge and Mo L<sub>3</sub>-edge XANES and Cr K-edge EXAFS measurements were performed at the Soft X-ray Microcharacterization Beamline (SXRMB) of the Canadian Light Source (CLS), Saskatoon, Canada. SXRMB is a bendingmagnet-based beamline that utilizes InSb(111) and Si(111) crystals for monochromatization to cover an energy range of 1.7-10 keV. Samples were mounted onto double-sided, conductive carbon tape and loaded into the vacuum chamber with a vacuum of 10<sup>-7</sup> Torr. Na<sub>2</sub>CrO<sub>4</sub> and HgSO<sub>4</sub> were used as references and for energy calibration. A 7-element SDD detector was used to record the fluorescence yield (FY) of the powder samples. The total electron yield (TEY) by recording the drain current of the sample was also recorded. The collected data were processed and analyzed using the Demeter software package including Athena and Artemis. 45 Data from multiple scans were processed using Athena by aligning and merging the spectra followed by background subtraction using the AUTOBK algorithm. Chromium K-edge EXAFS data analysis was conducted on the merged and normalized spectra using Artemis. Theoretical models were constructed with the program FEFF7. Cr<sub>2</sub>O<sub>3</sub> was used as a reference structural model.46 Fits to the Cr EXAFS data were made in R space (R from 1 to 3.2 Å) and obtained by taking the Fourier Transform (FT) of  $\chi(k)$  (k from 1.5 to 10.5) with a k weighting of 3.

## ■ RESULTS AND DISCUSSION

Synthesis and Characterization of LDH-Mo<sub>3</sub>S<sub>13</sub> Nanosheets. The LDH-Mo<sub>3</sub>S<sub>13</sub> hybrid nanosheets were synthesized using a novel two-step method starting from LDH-NO<sub>3</sub> that involves (i) the chemical exfoliation of LDH-

NO<sub>3</sub> and (ii) the subsequent treatment of the exfoliated ultrathin LDH nanosheets by the  $[Mo_3S_{13}]^{2-}$  anion (Figure 1). This modified synthesis is advantageous over the previously reported method<sup>36</sup> because it reduces ~90% of the organic solvents and the time to produce LDH-Mo<sub>3</sub>S<sub>13</sub>. A shorter interaction time in the solution can help to produce LDH nanosheets, retain the integrity of [Mo<sub>3</sub>S<sub>13</sub>]<sup>2-</sup> anions, and avoid the side reactions. SEM and TEM images reveal the platelike morphology of LDH-Mo<sub>3</sub>S<sub>13</sub> nanosheets (Figures 1A and 1B). EDS determines the average abundance of Mg, Al, Mo, and S is 20.8, 13.4, 12.4, and 53.4 in atomic percentage, respectively. Here, the Mo:S ratio is ~1:4.3 which is aligned to the composition of [Mo<sub>3</sub>S<sub>13</sub>]<sup>2-</sup> anions. Elemental mapping of SEM micrographs further confirms the uniform distributions of Mg, Al, Mo, and S across the LDH-Mo<sub>3</sub>S<sub>13</sub> crystallites (Figure S1). Infrared spectrum of the LDH-NO<sub>3</sub> shows a very strong peak at about 1370 cm<sup>-1</sup> that corresponds to the stretching vibration of  $NO_3^-$  anions,  $^{47,48}_{,48}$  while for LDH-Mo<sub>3</sub>S<sub>13</sub>, the intensity of the 1370 cm<sup>-1</sup> peak is markedly diminished (Figure 1C). This demonstrates the exchange of NO<sub>3</sub><sup>-</sup> with  $[Mo_3S_{13}]^{2-}$  anions between the positively charge nanosheets of

Sorption of CrO<sub>4</sub><sup>2-</sup> from Water. The sorption experiments with Cr6+ show that LDH-Mo<sub>3</sub>S<sub>13</sub> nanosheets are highly efficient for the sequestration of CrO<sub>4</sub><sup>2-</sup> from water under acidic, neutral, and alkaline conditions (Table S2). At neutral pH, from 1000 ppb of a Cr<sup>6+</sup> (CrO<sub>4</sub><sup>2-</sup>) spiked deionized water (DIW) solution, LDH-Mo<sub>3</sub>S<sub>13</sub> can capture over 99.99% of Cr6+ leaving the final concentration below 1 ppb with a  $K_d$  value of  $\sim 1.0 \times 10^7$  mL/g in 24 h (Tables S2 and S3). This concentration is well below the tolerance limits provided by the U.S. EPA (100 ppb) and WHO (50 ppb) for drinking water. 49,50 Also, it should be noted that the value of  $K_{\rm d}$  is higher to or comparable to other high performing materials known in the literature. At pH  $\sim$  11, LDH– Mo<sub>3</sub>S<sub>13</sub> can sequester over 98.7% of Cr<sup>6+</sup> decreasing the final concentration to 13 ppb with the  $K_{\rm d} \sim 7.7 \times 10^4$  mL/g in 48 h. Conversely, at pH  $\sim$  2, LDH-Mo<sub>3</sub>S<sub>13</sub> can sequester over 74% of Cr6+ ions. The lower effectiveness at this pH may be attributed to the slow decomposition of LDH-Mo<sub>3</sub>S<sub>13</sub>. A similar experiment with a 10-fold higher Cr<sup>6+</sup> concentration revealed similar adsorption efficiencies of over 79.2, 99.9, and 91.9% at pH  $\sim$  2, 7, and 11, respectively (Table S2). Noticeably, despite the 10-fold increase of Cr<sup>6+</sup> concentrations in the solutions, the residual concentrations, especially at neutral pH, remain below 10 ppb with  $K_d$  values of  $\geq 10^6$  mL/ g. Overall, our experiments show that LDH-Mo<sub>3</sub>S<sub>13</sub> is highly efficient to remove Cr6+ from neutral and alkaline media.

The kinetic study of LDH $-Mo_3S_{13}$  for the removal of  $Cr^{6+}$  was conducted using initial concentrations of  $1.0 \times 10^3$  and 1.0

× 10<sup>4</sup> ppb of Cr<sup>6+</sup> in DIW (Figures 2A and 2B, Tables S3 and S4). The experimental data were fitted with the pseudo-

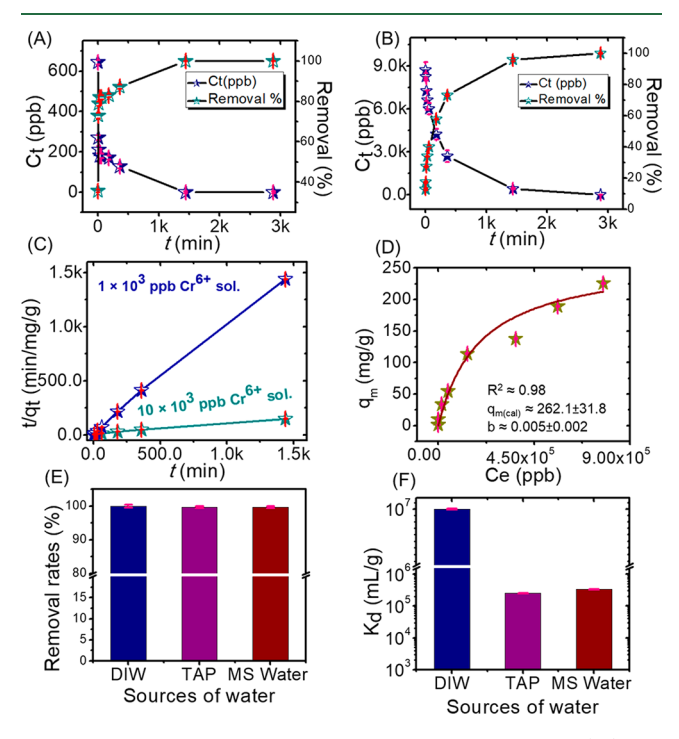


**Figure 2.** Adsorption kinetics for the residual concentrations  $(C_t)$  and removal rates of  $Cr^{6+}$  for  $1.0 \times 10^3$  ppb (A) and  $1.0 \times 10^4$  ppb (B) solutions in DIW; a comparison of the pseudo-second-order adsorption kinetics for  $1 \times 10^3$  and  $1 \times 10^4$  ppb solutions (C); adsorption capacity  $(q_m)$  vs equilibrium adsorption concentrations  $(C_e)$  (D); and a comparable study of the sorption of  $Cr^{6+}$  from CrO<sub>4</sub><sup>2-</sup> spiked DIW, Tap, and Mississippi River water showing the removal rate (E) and distribution coefficient (F). These experiments were conducted using 10 mg of LDH-Mo<sub>3</sub>S<sub>13</sub> in 10 mL  $(V/m \sim$ 1000 mL/g) of solutions at room temperature and pressure for a period of 48 h for (A-D) and 24 h for (E and F). The blue and bluegreen stars in A and B represent Ct and the removal percentage, respectively. In C, the blue and blue-green stars represent  $1.0 \times 10^3$ and  $1.0 \times 10^4$  ppb of Cr<sup>6+</sup> concentration; golden yellow stars in D represent equilibrium concentrations, and the red bars in A-F represent standard deviations.

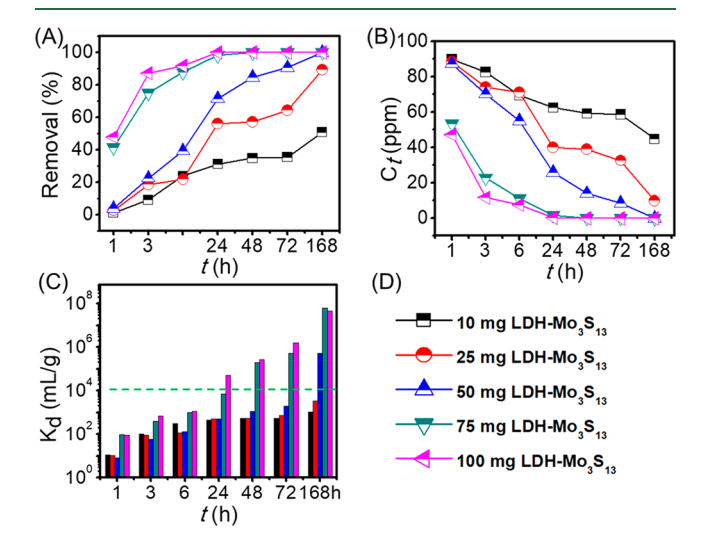
second-order rate equation that yielded the coefficient of determination,  $R^2 > 0.99$  (Figure 2C, Table S5). The pseudosecond-order rate constants were determined to be  $0.0886 \pm 0.0572$  and  $0.0015 \pm 0.0003$  g/mg·min<sup>-1</sup> for  $1.0 \times 10^3$  and  $1.0 \times 10^4$  ppb of Cr<sup>6+</sup> solutions, respectively. The difference in rate constants is indicative of different sorption mechanisms at different initial concentrations. Apart from this, the higher rate constant indicates faster sorption kinetics of Cr<sup>6+</sup> for the  $1.0 \times 10^3$  ppb solution.

To evaluate  $Cr^{6+}$  uptake capacity and adsorption isotherm, we investigated the sorption of  $Cr^{6+}$  for a broad range of concentrations,  $1.0 \times 10^3$  to  $1.0 \times 10^5$  ppb (Figure 2D, Table S6). This study reveals that the sorption capacity increases with the increase of  $Cr^{6+}$  concentrations until it reaches an equilibrium. Our experiment determines that the maximum adsorption of  $Cr^{6+}$  is about 225 mg/g. This value of sorption capacity is superior to other high performing materials, namely LDH $-MoS_4 \sim 130$  mg/g and  $CoAl-LDH \sim 93.5$  mg/g,  $^{18,24}$  cationic aluminum oxyhydroxides  $\sim 105.4$  mg/g,  $^{51}$  and anion exchange resin (IRN78  $\sim 63.5$  mg/g),  $^{51}$  and comparable to

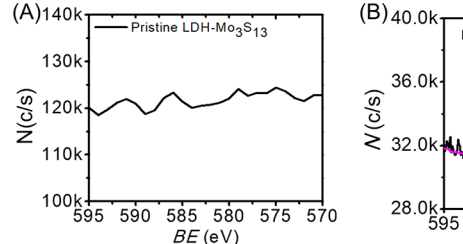
metal organic frameworks (MOR-1-HA  $\sim 242)^{52}$  and non-LDH cationic layered material (TJU-1  $\sim 279$  mg/g). <sup>26</sup> The experimentally obtained Cr<sup>6+</sup> sorption isotherm data are fitted with the Langmuir model which yielded  $R^2 \sim 0.98$  (Figure 2D). The Langmuir constant, b, was obtained as 0.005(2) L/mg and is comparable to other Cr<sup>6+</sup> adsorbents. <sup>53</sup>

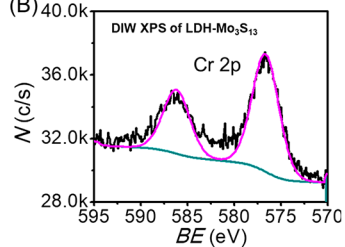
To determine the effectiveness of LDH-Mo<sub>3</sub>S<sub>13</sub> for Cr<sup>6+</sup> removal in the presence of highly competitive ions in purified and naturally contaminated water, we investigated Cr6+ removal efficiency from tap water and Mississippi River water (collected from Vidalia, Louisiana) by spiking them with 1000 ppb of Cr<sup>6+</sup> (CrO<sub>4</sub><sup>2-</sup>) (Figures 2E and 2F, Table S7). This study showed that despite the presence of numerous ions, such as Ca<sup>2+</sup>, Mg<sup>2+</sup>, Na<sup>+</sup>, K<sup>+</sup>, HCO<sub>3</sub><sup>-</sup>, SO<sub>4</sub><sup>2-</sup>, and Cl<sup>-</sup>, and other organic or inorganic constituents, LDH-Mo<sub>3</sub>S<sub>13</sub> can remove  $\geq$ 99.6% of  $Cr^{6+}$ . Such a high removal rate is indicative of the higher efficiency of LDH $-Mo_3S_{13}$  for  $CrO_4^{\ 2-}$  removal. Such an ultrahigh removal decreased its final concentration to <5 ppb with  $K_{\rm d} \sim 10^5$  mL/g. These values are close to the values obtained for DIW as discussed above. This finding suggests that LDH-Mo<sub>3</sub>S<sub>13</sub> is effective at sequestration of Cr<sup>6+</sup> even in the presence of highly competitive ions.

Removal of CrO<sub>4</sub><sup>2-</sup>, a Surrogate of TcO<sub>4</sub><sup>-</sup>, from the Simulated off-Gas Condensate of Hanford's LAW. To evaluate the removal efficiency of LDH-Mo<sub>3</sub>S<sub>13</sub> for chromate, a nonradiogenic surrogate of <sup>99</sup>TcO<sub>4</sub><sup>-</sup>, we investigated the simulated LAW melter off-gas condensate of Hanford's WTP (Figure 3, Tables S8-S12). The simulant was prepared following a procedure described by Taylor-Pashow et al.<sup>4,9</sup> The chemical composition of the simulant consists of high



**Figure 3.** Time-dependent sorption of  ${\rm CrO_4}^{2-}$  with an initial concentration of  $9.086 \times 10^4$  ppb of  ${\rm Cr^{6+}}$  as  ${\rm CrO_4}^{2-}$  ( ${\rm CrO_4}^{2-}$  equivalent concentrations  $\sim\!2.027 \times 10^5$  ppb) as a nonradioactive surrogate of  ${\rm TcO_4}^-$  from the simulated off-gas condensate of Hanford's LAW melter with respect to various amounts of loading of the sorbents showing the removal (%) of  ${\rm CrO_4}^{2-}$  (A), residual chromate concentration in the simulant (B), and the variation of  $K_{\rm d}$  (mL/g) (C). Panel (D) represents the symbols that demonstrate the various amounts of LDH– ${\rm Mo_3}S_{13}$  used for this experiment. These experiments were conducted using 10 mg of LDH– ${\rm Mo_3}S_{13}$  in 10 mL ( $V/m \sim 1000$  mL/g) of simulant solutions at room temperature and pressure for a period of 1 h through 68 h. Each experiment was replicated four times, and the average was considered to plot the diagram and analyze the results.





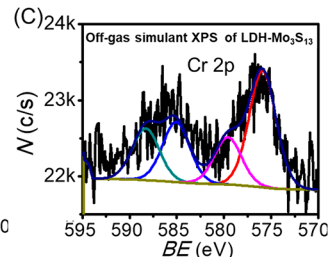


Figure 4. XPS spectra were collected for the pristine LDH-Mo<sub>3</sub>S<sub>13</sub> showing the absence of Cr (A), and the DIW XPS data (B) and the simulant XPS (C) show the presence of Cr. The DIW data was collected after the sorption experiments for  $1 \times 10^5$  ppb of Cr<sup>6+</sup> using 10 mg of LDH-Mo<sub>3</sub>S<sub>13</sub> in DIW, and the simulant XPS was collected for  $9.086 \times 10^4$  ppb of the Cr<sup>6+</sup> containing solution after treating the solutions using 100 mg of LDH-Mo<sub>3</sub>S<sub>13</sub>. Each experiment was conducted with 10 mL of solutions.

concentrations of anions, e.g., F<sup>-</sup>, Cl<sup>-</sup>, CO<sub>3</sub><sup>2-</sup>, NO<sub>3</sub><sup>-</sup>, BO<sub>3</sub><sup>3-</sup>, NO<sub>2</sub><sup>-</sup>, SO<sub>4</sub><sup>2-</sup>, and B<sub>4</sub>O<sub>7</sub><sup>2-</sup> at pH  $\sim$  7.5.

We observed that for the 10 and 25 mg loading of LDH- $Mo_3S_{13}$ , the maximum removal of  $Cr^{6+}$  was about 50.7 and 89.3%, respectively, from a  $9.086 \times 10^4$  ppb  $Cr^{6+}$  spiked simulated solution after 7 days of interactions (Figures 3A and 3B, Tables S8 and S9). This value of removal rate and  $K_d$  are remarkably higher than that of the LDH-NO3 and (NH<sub>4</sub>)<sub>2</sub>Mo<sub>3</sub>S<sub>13</sub>, suggesting the importance of the LDH-Mo<sub>3</sub>S<sub>13</sub> for the ultrahigh removal of Cr<sup>6+</sup> ions from the simulated solution (Table S13). Conversely, for an interaction of 50 mg of LDH-Mo<sub>3</sub>S<sub>13</sub>, the Cr<sup>6+</sup> removal reached >99.7% in 7 d. This leads to the residual concentration of  $\text{Cr}^{6+}$  to  ${\sim}35$ ppb and  $K_{\rm d}$  values of ~5 × 10<sup>5</sup> mL/g (Figure 3C, Table S10). With a higher loading of 75 and 100 mg of LDH-Mo<sub>3</sub>S<sub>13</sub>, the removal of Cr<sup>6+</sup> reached over 99.9 and 99.7% in only 2 and 1 d, respectively (Figure 3C, Tables S11 and S12). Importantly, after 3 days, the residual concentrations reach trace levels, 23 (75 mg) and 6 ppb (100 mg), and the  $K_d$  values reach  $\geq 10^5$ mL/g. Besides, after 7 d of exposure, removal percentages reach ~100%, residual concentrations become as low as <0.1 ppb, and the  $K_d$  reach  $\sim 10^7$  mL/g. Herewith, LDH-Mo<sub>3</sub>S<sub>13</sub> demonstrates itself as a highly efficient sorbent of CrO<sub>4</sub><sup>2-</sup> and by extension also its TcO<sub>4</sub><sup>-</sup> surrogate from the simulated offgas condensate of the LAW melter.

Understanding the Adsorption Mechanisms. The EDS and elemental mapping of the solid samples after the reaction with  ${\rm CrO_4}^{2-}$  in DIW and simulated solution show the presence chromium across the sorbents (Figures S2 and S3). The SEM and TEM images of the solid sorbents after the adsorption study show the retention of the platelike morphology (Figures S2 and S3). The TEM image of the postinteracted solids shows the presence of hexagonal crystallites similar to pristine LDH— ${\rm Mo_3S_{13}}$ . For the simulant treated samples, the crystallites' surface becomes deteriorated which could be the impact of highly concentrated anions of F<sup>-</sup>, Cl<sup>-</sup>, and others.

XPS analysis of the pristine and loaded LDH $-Mo_3S_{13}$  revealed the chemical state of the Mo, S, and Cr ions (Figure 4, Table S14). The post-treatment solid samples of LDH $-Mo_3S_{13}$  show the doublet of the peaks in the range of 570-595 eV corresponding to Cr 2p orbitals. As expected, these peaks are absent in the pristine LDH $-Mo_3S_{13}$ . Specifically, the postadsorbed samples in water show the peaks at 586.2 eV/576.7 eV corresponding to the Cr<sup>3+</sup> oxidation state, probably the formation of Cr<sub>2</sub>O<sub>3</sub>. Hence, the doublet of peaks is the result of the spin-orbit splitting of the Cr<sup>3+</sup> 2p orbitals. <sup>18,54</sup> For the samples that were treated with simulated solutions, the XPS show two pairs of peaks at 577.5 eV/585.5 and 589.1 eV/579.5 eV. The bands at 577.5 eV/585.5 eV can be originated

from  $Cr^{3+}$ , while the peaks at higher energy are attributed to  $Cr^{6+}$  ions of the  $CrO_4^{2-}.^{54,55}$  The S 2p peaks that are observed in the range of 169.2-171.2 eV can be attributed to the oxidation of sulfides to sulfate anions (Figure S4). Similarly, for the Mo 3d, the weak peaks that are observed at about 236 eV are the results of the partial oxidation of  $Mo^{4+}$  to  $Mo^{6+}$  of the  $Mo^{4+}{}_3S_{13}$  moieties of LDH $-Mo_3S_{13}$  (Figure S4).  $^{59,60}$ 

Furthermore, ICP analysis shows the presence of molybdenum ions in the postinteraction solutions. A quantitative analysis by ICP MS determined that  $\sim\!\!21\%$  of Mo of LDH— $Mo_3S_{13}$  dissolves. The presence of molybdenum ions can be attributed to oxidation dissolution of  $Mo^{4+}$  of the  $[Mo^{4+}_3S_{13}]^{2-}$  to  $Mo^{6+}$  ions. The dissolution of  $Mo^{6+}$  results in the concurrent dissolution of sulfide which is likely to oxidize to sulfate/sulfite anions. Hence, this study reveals that a cooperative oxidation of both sulfur and molybdenum likely enhances the reduction of  $Cr^{6+}$  to  $Cr^{3+}$ .

The Cr K-edge XANES spectra of LDH-Mo<sub>3</sub>S<sub>13</sub> samples were collected after reaction with CrO<sub>4</sub><sup>2-</sup> in DIW and the simulated LAW off-gas condensate, together with Na<sub>2</sub>CrO<sub>4</sub> as a model compound (Figure 5A). For Na<sub>2</sub>CrO<sub>4</sub>, a sharp edge peak at 5994.0 eV is observed which is characteristic of the four coordinated character of the hexavalent chromate ion (CrO<sub>4</sub><sup>2-</sup>).<sup>61,62</sup> Conversely, this peak at 5994.0 eV nearly completely disappeared for the DIW interacted sample, suggesting that Cr6+ was hardly detectable and the dominant species was  $Cr^{3+}$  reduced from  $CrO_4^{\ 2-}$ . Additionally, there was another weak peak at 5991.2 eV, which is a typical pre-edge peak for  $Cr_2O_3$  or  $Cr(OH)_3$ . The solid sorbent obtained from the simulant experiment shows the presence of the peak at 5994.0 eV representative of CrO<sub>4</sub><sup>2-</sup> ions. It is estimated from the Cr K-edge XANES there is  $\sim 15\%$  CrO<sub>4</sub><sup>2-</sup> and  $\sim 85\%$ Cr<sup>3+</sup> in this sample. In addition, there was a new peak at 5988.2 eV, together with a bump at 5991.2 eV corresponding to the pre-edge peak observed for the DIW treated sorbent. These two features are attributed to the split of the pre-edge and are assigned to Cr 1s transitions to 3d  $(t_{2g})$  and 3d  $(e_g)$  electronic states, respectively, in the polyhedra of  $Cr^{3+}$  ions. <sup>64</sup> Overall, the Cr K-edge of XANES spectra of Na<sub>2</sub>CrO<sub>4</sub> and postinteracted LDH-Mo<sub>3</sub>S<sub>13</sub> in DIW and the simulant illustrate features that are consistent with the Cr valence state and change in coordination number. Notably, the reductive precipitation of  $Cr^{6+} \rightarrow Cr^{3+}$  could be attributed to the presence of highly redox active sulfide anions in LDH-Mo<sub>3</sub>S<sub>13</sub>. Hence, the higher redox potentials of  $Tc^{7+}$  ( $TcO_4^-/Tc^{4+}$  is  $E^{\circ} \sim +0.74$  V)<sup>21</sup> and  $Cr^{6+}$  ( $CrO_4^{2-}/Cr^{3+}$  is  $E^{\circ} \sim +1.23$  V)<sup>20</sup> enable their reduction by the mono- and disulfides species,  $S^{2/1-} \rightarrow S^{n+} + ne^-$  (e.g.,  $E^{\circ}$ of  $S^{2-}/SO_4^{2-}$  is  $\sim -0.22$  V), of LDH-Mo<sub>3</sub>S<sub>13</sub>. This

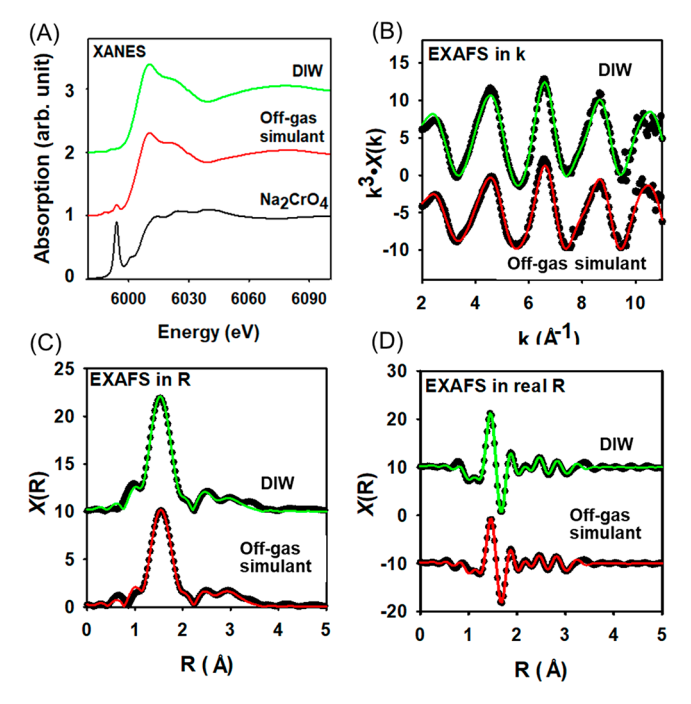


**Figure 5.** Cr K-edge XANES and EXAFS spectra of two LDH— $Mo_3S_{13}$  samples after Cr treatments in DIW and an off-gas simulant, XANES, together with the spectrum of  $Na_2CrO_4$  (A), EXAFS data in k space (B), EXAFS data in R space (C), and EXAFS data in real R space (D). Dotted and solid-colored lines in EXAFS represent experimental and fitted data, respectively.

reduction immobilizes  $Tc^{4+}/Cr^{3+}$  salts by the deposition of technetium and chromium containing solids on the sorbent. Since this reductive precipitation is the dominant mechanism for the sequestration of  $Cr^{6+}$  and the sorbents are contaminated with the precipitated solids, this material is unlikely to be reusable.

XPS and XANES predominantly show the removal of chromium involves reduction of Cr<sup>6+</sup> to Cr<sup>3+</sup>. The CrO<sub>4</sub><sup>2-</sup> anion adopts a tetrahedral geometry, while the Cr<sup>3+</sup> species remains predominantly in an octahedrally coordinated environment. This change in coordination number and the geometry are further demonstrated by Cr K-edge EXAFS data (Figure 5B–D). The fitted EXAFS parameters of these samples are summarized in Table 1, in comparison with the X-ray

diffraction data of Cr<sub>2</sub>O<sub>3</sub>. The Cr K-edge EXAFS data of the sorbent sample exposed to CrO<sub>4</sub><sup>2-</sup> in DIW was fitted with octahedral Cr-O paths at a Cr-O distance of 1.971  $\pm$  0.005 Å with a fitted coordination number of 5.10  $\pm$  0.39 and three Cr-Cr paths at  $2.54 \pm 0.03$ ,  $3.09 \pm 0.03$ , and  $3.38 \pm 0.03$  Å, respectively, with the corresponding fixed coordination numbers obtained from Cr<sub>2</sub>O<sub>3</sub> X-ray diffraction data.<sup>46</sup> The Cr-O octahedron in Cr<sub>2</sub>O<sub>3</sub> displays three Cr-O bonds at a distance of 1.964 Å and three Cr-O bonds at a distance of 2.013 Å, but the EXAFS data fitting was kept with the same Cr-O bond distance to limit the fitting parameters. The fitted Cr-O bond distance of 1.971 Å and the coordination number of 5.1 are comparable to those in Cr<sub>2</sub>O<sub>3</sub>, but the fitted bond distances for two of three Cr-Cr paths show a larger variation compared to those in Cr2O3. However, the overall EXAFS data fitting of this sample was acceptable as measured by the R factor of 0.0026 (Table 1). Thus, the Cr K-edge EXAFS spectra of the sorbent exposed to CrO<sub>4</sub><sup>2-</sup> in DIW confirmed that the Cr species associated with the sorbent was likely  $Cr_2O_3$  or  $Cr(OH)_3$ .

The Cr K-edge EXAFS data of the sorbent sample exposed to CrO<sub>4</sub><sup>2-</sup> in the off-gas simulant was also fitted using the Cr<sub>2</sub>O<sub>3</sub> structure model. Although its Cr K-edge XANES indicated that 15.4% of Cr was CrO<sub>4</sub><sup>2-</sup>, the EXAFS data fitting did not permit more parameters with the addition of another phase. In general, the fitted EXAFS parameters for the sorbent exposed to  ${\rm CrO_4}^{2-}$  in the off-gas simulant were similar to those of the sorbent exposed to CrO<sub>4</sub><sup>2-</sup> in DIW (Table 1), and the overall fitting of this sample was acceptable as measured by the R factor of 0.0039 (Table 1). However, the fitted Cr-O coordination number for this sample was  $3.72 \pm 0.35$  (Table 1), which was significantly smaller than the Cr-O coordination number of 5.1 in the sample retrieved from DIW and the Cr-O coordination number of 6 in Cr<sub>2</sub>O<sub>3</sub>. Except for the common error of up to 20% for the fitted coordination number from the EXAFS data fitting, this discrepancy might also indicate that a small portion of Cr in this sample was tetrahedral CrO<sub>4</sub><sup>2-</sup>. Thus, the Cr K-edge EXAFS spectra of the sorbent exposed to CrO<sub>4</sub><sup>2-</sup> in the off-gas simulant confirmed that the dominant Cr species associated with the sorbent was likely Cr<sub>2</sub>O<sub>3</sub> or Cr(OH)<sub>3</sub>, but a small amount of CrO<sub>4</sub><sup>2-</sup> was also present, consistent with its Cr K-edge XANES data discussed above.

Table 1. Cr K-Edge Fitting Data for the Cr Species after Interactions of LDH $-Mo_3S_{13}$  with  $CrO_4^{\ 2^-}$  in Water and in the Simulated LAW off-Gas Condensate

samples	path	bond distance (Å)	coordination number	Debye–Waller factor, $\sigma$ 2 (Å2)	$\Delta E0~(\mathrm{eV})$	R-factor
DIW	Cr-O2	$1.971 \pm 0.005$	$5.10 \pm 0.39$	$0.0026 \pm 0.0007$	$3.2 \pm 0.8$	0.0026
	Cr-Cr1	$2.54 \pm 0.03$	1	$0.0149 \pm 0.0047$		
	Cr-Cr2	$3.09 \pm 0.03$	3	$0.0155 \pm 0.0039$		
	Cr-Cr3	$3.38 \pm 0.03$	3	$0.0111 \pm 0.0027$		
off-gas simulant	Cr-O2	$1.976 \pm 0.005$	$3.72 \pm 0.35$	$0.0011 \pm 0.0009$	$3.7 \pm 1.0$	0.0039
	Cr-Cr1	$2.56 \pm 0.05$	1	$0.0185 \pm 0.0072$		
	Cr-Cr2	$3.09 \pm 0.05$	3	$0.0216 \pm 0.0072$		
	Cr-Cr3	$3.39 \pm 0.02$	3	$0.0108 \pm 0.0025$		
$Cr_2O_3$	Cr-O1	1.964	3			
	Cr-O2	2.013	3			
	Cr-Cr1	2.650	1			
	Cr-Cr2	2.888	3			
	Cr-Cr3	3.425	3			

Mo L3-edge XANES reveals the presence of the dipole allowed  $2p \rightarrow 4d$  transition of  $Mo^{4+}$  at 2523.8 eV, indicating that Mo predominantly remains as  $Mo^{4+}$  in the postreacted solids, in agreement with XPS results (Figure S5). The XANES of S K-edge shows peaks at about 2471.4, 2471.6, and 2471.7 eV for the pristine, water, and simulant treated samples, respectively. These peaks demonstrate the presence of sulfide species. The peak at 2481.9 eV can be ascribed to  $S^{6+}$  oxidation states which suggests concomistant oxidation of some of the sulfide groups of LDH $-Mo_3S_{13}$ . Importantly, the intensity of the  $S^{6+}$  peaks sharply increases from the pristine to the simulant treated LDH $-Mo_3S_{13}$ , indicating a higher propensity of sulfide oxidation in the simulated solutions which further supports the reductive precipitation of  $Cr^{6+}$  to  $Cr^{3+}$ .

Altogether, an insight of the sorption mechanisms demonstrates that reductive precipitation is the dominant mechanism for the removal of  ${\rm TcO_4}^-/{\rm CrO_4}^{2-}$ ; nevertheless, a small contribution of ion-exchange and/or surface adsorption cannot be ruled out, especially for the simulated off-gas condensate of the LAW melter. The reductive precipitation mechanism requires the use of  $S^{n-}$  (n=1,2) and  ${\rm Mo^{4+}}$  of the LDH- ${\rm Mo_3S_{13}}$  as the reductants to precipitate out the  ${\rm Cr^{3+}}$  species. Overall, this study reveals that LDH- ${\rm Mo_3S_{13}}$  is a high performing sorbent of  ${\rm TcO_4}^-/{\rm CrO_4}^{2-}$  from defense nuclear legacy waste. We believe this finding advances our knowledge and points to design principles of materials that can accomplish excellent efficiency in complex high ionic strength solutions for the sequestration of pertechnetate and chromate anions from aqueous solutions.

### ASSOCIATED CONTENT

#### **Supporting Information**

The Supporting Information is available free of charge at https://pubs.acs.org/doi/10.1021/acs.est.1c08766.

Details on uptake study as well as characterization of pristine and postadsorption LDH-Mo<sub>3</sub>S<sub>13</sub> (PDF)

## AUTHOR INFORMATION

#### **Corresponding Author**

Saiful M. Islam – Department of Chemistry, Physics, and Atmospheric Sciences, Jackson State University, Jackson, Mississippi 39217, United States; oocid.org/0000-0001-8518-1856; Email: muhammad.s.islam@jsums.edu

#### **Authors**

Ahmet Celik – Department of Chemistry, Physics, and Atmospheric Sciences, Jackson State University, Jackson, Mississippi 39217, United States

Dien Li – Savannah River National Laboratory, Aiken, South Carolina 29808, United States

Michael A. Quintero — Department of Chemistry, Northwestern University, Evanston, Illinois 60208, United States; © orcid.org/0000-0002-0709-1676

Kathryn M. L. Taylor-Pashow — Savannah River National Laboratory, Aiken, South Carolina 29808, United States; orcid.org/0000-0002-1986-0866

Xianchun Zhu — Department of Civil Engineering, Jackson State University, Jackson, Mississippi 39217, United States Mohsen Shakouri — Canadian Light Source, Saskatoon, Saskatchewan S7N 0X4, Canada

- Subrata Chandra Roy Department of Chemistry, Physics, and Atmospheric Sciences, Jackson State University, Jackson, Mississippi 39217, United States
- Mercouri G. Kanatzidis Department of Chemistry, Northwestern University, Evanston, Illinois 60208, United States; occid.org/0000-0003-2037-4168
- Zikri Arslan Department of Chemistry, Physics, and Atmospheric Sciences, Jackson State University, Jackson, Mississippi 39217, United States
- Alicia Blanton Department of Chemistry, Physics, and Atmospheric Sciences, Jackson State University, Jackson, Mississippi 39217, United States
- Jing Nie Department of Chemistry, Physics, and Atmospheric Sciences, Jackson State University, Jackson, Mississippi 39217, United States
- Shulan Ma College of Chemistry, Beijing Normal University, Beijing 100875, China; orcid.org/0000-0002-8326-3134
- Fengxiang X. Han Department of Chemistry, Physics, and Atmospheric Sciences, Jackson State University, Jackson, Mississippi 39217, United States; orcid.org/0000-0001-5135-3031

Complete contact information is available at: https://pubs.acs.org/10.1021/acs.est.1c08766

#### **Notes**

Any use of trade, firm, or product names is for descriptive purposes only and does not imply endorsement by the U.S. Government.

The authors declare no competing financial interest.

### ACKNOWLEDGMENTS

This work was partially supported by the US Department of Energy Minority Serving Institution Partnership Program (MSIPP) managed by the Savannah River National Laboratory under SRNS contract (RFP No. 0000542525 and 0000458357). S.C.R. is thankful to the NSF Division of Chemistry (NSF-2100797). All of the ICP-MS analysis was conducted at JSU's core research centers supported by RCMI (NIH grant: 1U54MD015929). X-ray Absorption Spectroscopy was performed at the SXRMB beamline of the Canadian Light Source, a national research facility of the University of Saskatchewan, which is supported by the Canada Foundation for Innovation (CFI), the Natural Sciences and Engineering Research Council (NSERC), the National Research Council (NRC), the Canadian Institutes of Health Research (CIHR), the Government of Saskatchewan, and the University of Saskatchewan. This work made use of the Keck-II facility of Northwestern University's NUANCE Center, which has received support from the SHyNE Resource (NSF ECCS-2025633), the IIN, and Northwestern's MRSEC program (NSF DMR-1720139).

#### REFERENCES

- (1) Taylor-Pashow, K. M. L.; Poirier, M.; McCabe, D. J. Bench Scale Experiments for the Remediation of Hanford Waste Treatment Plant Low Activity Waste Melter Off-Gas Condensate; SRNL-STI-2017-00322; Savannah River Site (SRS): Aiken, SC, United States, 2017; DOI: 10.2172/1377029.
- (2) Wilmarth, W. R.; Lumetta, G. J.; Johnson, M. E.; Poirier, M. R.; Thompson, M. C.; Suggs, P. C.; Machara, N. P. Review: Waste-Pretreatment Technologies for Remediation of Legacy Defense Nuclear Wastes. *Solvent Extr. Ion Exch.* **2011**, 29 (1), 1–48.

- (3) Adamson, D. J.; Nash, C. A.; McCabe, D. J.; Crawford, C. L.; Wilmarth, W. R. Laboratory Evaporation Testing Of Hanford Waste Treatment Plant Low Activity Waste Off-Gas Condensate Simulant; SRNL-STI-2013-00713, 1117838; 2014; DOI: 10.2172/1117838.
- (4) Taylor-Pashow, K. M.; Nash, C. A.; Crawford, C. L.; McCabe, D. J.; Wilmarth, W. R. Laboratory Scoping Tests Of Decontamination Of Hanford Waste Treatment Plant Low Activity Waste Off-Gas Condensate Simulant; SRNL-STI-2013-00719; Savannah River Site (SRS): Aiken, SC, United States, 2014; DOI: 10.2172/1116991.
- (5) McCloy, J. S.; Riley, B. J.; Goel, A.; Liezers, M.; Schweiger, M. J.; Rodriguez, C. P.; Hrma, P.; Kim, D.-S.; Lukens, W. W.; Kruger, A. A. Rhenium Solubility in Borosilicate Nuclear Waste Glass: Implications for the Processing and Immobilization of Technetium-99. *Environ. Sci. Technol.* **2012**, *46* (22), 12616–12622.
- (6) Neeway, J. J.; Asmussen, R. M.; Lawter, A. R.; Bowden, M. E.; Lukens, W. W.; Sarma, D.; Riley, B. J.; Kanatzidis, M. G.; Qafoku, N. P. Removal of TcO<sub>4</sub><sup>--</sup> from Representative Nuclear Waste Streams with Layered Potassium Metal Sulfide Materials. *Chem. Mater.* **2016**, 28 (11), 3976–3983.
- (7) Pearce, C. I.; Moore, R. C.; Morad, J. W.; Asmussen, R. M.; Chatterjee, S.; Lawter, A. R.; Levitskaia, T. G.; Neeway, J. J.; Qafoku, N. P.; Rigali, M. J.; Saslow, S. A.; Szecsody, J. E.; Thallapally, P. K.; Wang, G.; Freedman, V. L. Technetium Immobilization by Materials through Sorption and Redox-Driven Processes: A Literature Review. Sci. Total Environ. 2020, 716, 132849.
- (8) Banerjee, D.; Kim, D.; Schweiger, M. J.; Kruger, A. A.; Thallapally, P. K. Removal of TcO<sub>4</sub><sup>-</sup> Ions from Solution: Materials and Future Outlook. *Chem. Soc. Rev.* **2016**, 45 (10), 2724–2739.
- (9) Taylor-Pashow, K. M. L.; McCabe, D. J.; Nash, C. A. Tc Removal from the Waste Treatment and Immobilization Plant Low-Activity Waste Vitrification off-Gas Recycle. *Sep. Sci. Technol.* **2018**, 53 (12), 1925–1934.
- (10) Sheng, D.; Zhu, L.; Xu, C.; Xiao, C.; Wang, Y.; Wang, Y.; Chen, L.; Diwu, J.; Chen, J.; Chai, Z.; Albrecht-Schmitt, T.; Wang, S. Efficient and Selective Uptake of  $TcO_4^-$  by a Cationic Metal-Organic Framework Material with Open Ag+ Sites. *Environ. Sci. Technol.* **2017**, *51*, 3471.
- (11) Pierce, E. M.; Mattigod, S. V.; Westsik, J. H.; Serne, R. J.; Icenhower, J. P.; Scheele, R. D.; Um, W.; Qafoku, N. Review of Potential Candidate Stabilization Technologies for Liquid and Solid Secondary Waste Streams; PNNL-19122; Pacific Northwest National Lab. (PNNL) and Environmental Molecular Sciences Lab. (EMSL): Richland, WA, United States, 2010; DOI: 10.2172/978974.
- (12) Hrma, P. R. Retention of Halogens in Waste Glass; PNNL-19361, 981571; 2010; DOI: 10.2172/981571.
- (13) Goel, A.; McCloy, J. S.; Pokorny, R.; Kruger, A. A. Challenges with Vitrification of Hanford High-Level Waste (HLW) to Borosilicate Glass An Overview. *J. Non Cryst. Solids* **2019**, *4*, 100033.
- (14) Johnson, F.; Stone, M.; McCabe, D. Evaluation of Immobilizing Secondary Waste from a Proposed Treatment Process for Hanford WTP LAW Melter Condensate; Savannah River Site (SRS): Aiken, SC, United States, 2018; DOI: 10.2172/1431111.
- (15) Pearce, C. I.; Moore, R. C.; Morad, J. W.; Asmussen, R. M.; Chatterjee, S.; Lawter, A. R.; Levitskaia, T. G.; Neeway, J. J.; Qafoku, N. P.; Rigali, M. J.; Saslow, S. A.; Szecsody, J. E.; Thallapally, P. K.; Wang, G.; Freedman, V. L. Technetium Immobilization by Materials through Sorption and Redox-Driven Processes: A Literature Review. Sci. Total Environ. 2020, 716, 132849.
- (16) Pearce, C. I.; Cordova, E. A.; Garcia, W. L.; Saslow, S. A.; Cantrell, K. J.; Morad, J. W.; Qafoku, O.; Matyáš, J.; Plymale, A. E.; Chatterjee, S.; Kang, J.; Colon, F. C.; Levitskaia, T. G.; Rigali, M. J.; Szecsody, J. E.; Heald, S. M.; Balasubramanian, M.; Wang, S.; Sun, D. T.; Queen, W. L.; Bontchev, R.; Moore, R. C.; Freedman, V. L. Evaluation of Materials for Iodine and Technetium Immobilization through Sorption and Redox-Driven Processes. *Sci. Total Environ.t* 2020, 716, 136167.
- (17) Wharton, M. J.; Atkins, B.; Charnock, J. M.; Livens, F. R.; Pattrick, R. A. D.; Collison, D. An X-Ray Absorption Spectroscopy

- Study of the Coprecipitation of Tc and Re with Mackinawite (FeS). *Appl. Geochem.* **2000**, *15* (3), 347–354.
- (18) Ma, L.; Islam, S. M.; Liu, H.; Zhao, J.; Sun, G.; Li, H.; Ma, S.; Kanatzidis, M. G. Selective and Efficient Removal of Toxic Oxoanions of As(III), As(V), and Cr(VI) by Layered Double Hydroxide Intercalated with MoS<sub>4</sub><sup>2--</sup>. *Chem. Mater.* **2017**, 29 (7), 3274–3284.
- (19) Pan, J.; Liu, L.; Pan, H.; Yang, L.; Su, M.; Wei, C. A Feasibility Study of Metal Sulfide (FeS and MnS) on Simultaneous Denitrification and Chromate Reduction. *J. Hazard. Mater.* **2022**, 424, 127491.
- (20) Liu, H.; Yu, X. Hexavalent Chromium in Drinking Water: Chemistry, Challenges and Future Outlook on Sn(II)- and Photocatalyst-Based Treatment. Front. Environ. Sci. Eng. 2020, 14 (5), 88.
- (21) Maset, E. R.; Sidhu, S. H.; Fisher, A.; Heydon, A.; Worsfold, P. J.; Cartwright, A. J.; Keith-Roach, M. J. Effect of Organic Co-Contaminants on Technetium and Rhenium Speciation and Solubility under Reducing Conditions. *Environ. Sci. Technol.* **2006**, 40 (17), 5472–5477.
- (22) Kim, J.; Jung, P.-K.; Moon, H.-S.; Chon, C.-M. Reduction of Hexavalent Chromium by Pyrite-Rich Andesite in Different Anionic Solutions. *Env. Geol.* **2002**, *42* (6), 642–648.
- (23) Pearce, C. I.; Icenhower, J. P.; Asmussen, R. M.; Tratnyek, P. G.; Rosso, K. M.; Lukens, W. W.; Qafoku, N. P. Technetium Stabilization in Low-Solubility Sulfide Phases: A Review. *ACS Earth Space Chem.* **2018**, 2 (6), 532–547.
- (24) Rathore, E.; Maji, K.; Biswas, K. Nature-Inspired Coral-like Layered [Co<sub>0.79</sub>Al<sub>0.21</sub>(OH)<sub>2</sub>(CO<sub>3</sub>)<sub>0.11</sub>]·mH<sub>2</sub>O for Fast Selective Ppb Level Capture of Cr(VI) from Contaminated Water. *Inorg. Chem.* **2021**, *60* (13), 10056–10063.
- (25) Ginder-Vogel, M.; Borch, T.; Mayes, M. A.; Jardine, P. M.; Fendorf, S. Chromate Reduction and Retention Processes within Arid Subsurface Environments. *Environ. Sci. Technol.* **2005**, 39 (20), 7833–7839.
- (26) Yang, H.; Fei, H. Exfoliation of a Two-Dimensional Cationic Inorganic Network as a New Paradigm for High-Capacity CrVI-Anion Capture. *Chem. Commun.* **2017**, *53* (52), 7064–7067.
- (27) Sylvester, P.; Rutherford, L. A.; Gonzalez-Martin, A.; Kim, J.; Rapko, B. M.; Lumetta, G. J. Ferrate Treatment for Removing Chromium from High-Level Radioactive Tank Waste. *Environ. Sci. Technol.* **2001**, 35 (1), 216–221.
- (28) Daily, W.; Ramirez, A.; Binley, A. Remote Monitoring of Leaks in Storage Tanks Using Electrical Resistance Tomography: Application at the Hanford Site. *JEEG* **2004**, *9* (1), 11–24.
- (29) Routson, R. C.; Price, W. H.; Brown, D. J.; Fecht, K. R. High-Level Waste Leakage from the 241-T-106 Tank at Hanford; No. RHO-ST-14; Rockwell International Corp.: Richland, WA, USA, 1979.
- (30) Zhao, H.; Deng, Y.; Harsh, J. B.; Flury, M.; Boyle, J. S. Alteration of Kaolinite to Cancrinite and Sodalite by Simulated Hanford Tank Waste and Its Impact on Cesium Retention. *Clays Clay Miner.* **2004**, 52 (1), 1–13.
- (31) Samanta, P.; Chandra, P.; Dutta, S.; Desai, A. V.; Ghosh, S. K. Chemically Stable Ionic Viologen-Organic Network: An Efficient Scavenger of Toxic Oxo-Anions from Water. *Chem. Sci.* **2018**, 9 (40), 7874–7881.
- (32) Fan, D.; Anitori, R. P.; Tebo, B. M.; Tratnyek, P. G.; Lezama Pacheco, J. S.; Kukkadapu, R. K.; Engelhard, M. H.; Bowden, M. E.; Kovarik, L.; Arey, B. W. Reductive Sequestration of Pertechnetate (<sup>99</sup>TcO<sub>4</sub><sup>--</sup>) by Nano Zerovalent Iron (NZVI) Transformed by Abiotic Sulfide. *Environ. Sci. Technol.* **2013**, *47* (10), 5302–5310.
- (33) Strickert, R.; Friedman, A. M.; Fried, S. The Sorption of Technetium and Iodine Radioisotopes by Various Minerals. *Nucl. Technol.* **1980**, *49* (2), 253–266.
- (34) Huie, Z.; Jishu, Z.; Lanying, Z. Sorption of Radionuclides Technetium and Iodine on Minerals. *Radiochim. Acta* **1988**, 44–45 (1), 143–146.
- (35) Wang, Y.; Gao, H. Compositional and Structural Control on Anion Sorption Capability of Layered Double Hydroxides (LDHs). *J. Colloid Interface Sci.* **2006**, 301 (1), 19–26.

- (36) Yang, L.; Xie, L.; Chu, M.; Wang, H.; Yuan, M.; Yu, Z.; Wang, C.; Yao, H.; Islam, S. M.; Shi, K.; Yan, D.; Ma, S.; Kanatzidis, M. G. Mo<sub>3</sub>S<sub>13</sub><sup>2-</sup> Intercalated Layered Double Hydroxide: Highly Selective Removal of Heavy Metals and Simultaneous Reduction of Ag<sup>+</sup> Ions to Metallic Ag<sup>0</sup> Ribbons. *Angew. Chem.* **2021**, *134* (1), e202112511.
- (37) Celik, A.; Baker, D. R.; Arslan, Z.; Zhu, X.; Blanton, A.; Nie, J.; Yang, S.; Ma, S.; Han, F. X.; Islam, S. M. Highly Efficient, Rapid, and Concurrent Removal of Toxic Heavy Metals by the Novel 2D Hybrid LDH-[Sn,S<sub>6</sub>]. Chem. Eng. J. 2021, 426, 131696.
- (38) Ma, S.; Fan, C.; Du, L.; Huang, G.; Yang, X.; Tang, W.; Makita, Y.; Ooi, K. Intercalation of Macrocyclic Crown Ether into Well-Crystallized LDH: Formation of Staging Structure and Secondary Host-Guest Reaction. *Chem. Mater.* **2009**, *21* (15), 3602–3610.
- (39) Islam, S. M.; Cain, J. D.; Shi, F.; He, Y.; Peng, L.; Banerjee, A.; Subrahmanyam, K. S.; Li, Y.; Ma, S.; Dravid, V. P.; Grayson, M.; Kanatzidis, M. G. Conversion of Single Crystal (NH<sub>4</sub>)<sub>2</sub>Mo<sub>3</sub>S<sub>13</sub>·H<sub>2</sub>O to Isomorphic Pseudocrystals of MoS<sub>2</sub> Nanoparticles. *Chem. Mater.* **2018**, *30* (11), 3847–3853.
- (40) Islam, S. M.; Sangwan, V. K.; Li, Y.; Kang, J.; Zhang, X.; He, Y.; Zhao, J.; Murthy, A.; Ma, S.; Dravid, V. P.; Hersam, M. C.; Kanatzidis, M. G. Abrupt Thermal Shock of (NH<sub>4</sub>)<sub>2</sub>Mo<sub>3</sub>S<sub>13</sub> Leads to Ultrafast Synthesis of Porous Ensembles of MoS<sub>2</sub> Nanocrystals for High Gain Photodetectors. *ACS Appl. Mater. Interfaces* **2018**, *10* (44), 38193–38200.
- (41) Manos, M. J.; Ding, N.; Kanatzidis, M. G. Layered Metal Sulfides: Exceptionally Selective Agents for Radioactive Strontium Removal. *Proc. Natl. Acad. Sci. U.S.A.* **2008**, *105* (10), 3696–3699.
- (42) Freundlich, H. Über die Adsorption in Lösungen. Zeitschrift für Physikalische Chemie 1907, 57U (1), 385–470.
- (43) Liu, T.; Yang, M.; Wang, T.; Yuan, Q. Prediction Strategy of Adsorption Equilibrium Time Based on Equilibrium and Kinetic Results To Isolate Taxifolin. *Ind. Eng. Chem. Res.* **2012**, *51* (1), 454–463.
- (44) Langmuir, I. THE ADSORPTION OF GASES ON PLANE SURFACES OF GLASS, MICA AND PLATINUM. *J. Am. Chem. Soc.* **1918**, 40 (9), 1361–1403.
- (45) Ravel, B.; Newville, M. ATHENA, ARTEMIS, HEPHAESTUS: Data Analysis for X-Ray Absorption Spectroscopy Using IFEFFIT. *J. Synchrotron Radiat.* **2005**, *12* (4), 537–541.
- (46) Sawada, H. Residual Electron Density Study of Chromium Sesquioxide by Crystal Structure and Scattering Factor Refinement. *Mater. Res. Bull.* **1994**, 29 (3), 239–245.
- (47) Ma, S.; Chen, Q.; Li, H.; Wang, P.; Islam, S. M.; Gu, Q.; Yang, X.; Kanatzidis, M. G. Highly Selective and Efficient Heavy Metal Capture with Polysulfide Intercalated Layered Double Hydroxides. *J. Mater. Chem. A* **2014**, 2 (26), 10280–10289.
- (48) Ma, S.; Shim, Y.; Islam, S. M.; Subrahmanyam, K. S.; Wang, P.; Li, H.; Wang, S.; Yang, X.; Kanatzidis, M. G. Efficient Hg Vapor Capture with Polysulfide Intercalated Layered Double Hydroxides. *Chem. Mater.* **2014**, *26* (17), 5004–5011.
- (49) US EPA O. Chromium in drinking water; US EPA: https://www.epa.gov/sdwa/chromium-drinking-water. https://19january2017snapshot.epa.gov/dwstandardsregulations/chromium-drinking-water (accessed 2021-12-12).
- (50) World Health Organization. *Guidelines for Drinking-Water Quality: Second Addendum; WHO:* 2008, 3rd ed.; World Health Organization: Geneva, 2008. https://www.who.int/publications/i/item/9789241547604 (accessed 2022-05-23).
- (51) Bai, P.; Dong, Z.; Wang, S.; Wang, X.; Li, Y.; Wang, Y.; Ma, Y.; Yan, W.; Zou, X.; Yu, J. A Layered Cationic Aluminum Oxyhydroxide as a Highly Efficient and Selective Trap for Heavy Metal Oxyanions. *Angew. Chem., Int. Ed.* **2020**, *59* (44), 19539–19544.
- (\$2) Rapti, S.; Pournara, A.; Sarma, D.; Papadas, I. T.; Armatas, G. S.; Tsipis, A. C.; Lazarides, T.; Kanatzidis, M. G.; Manos, M. J. Selective Capture of Hexavalent Chromium from an Anion-Exchange Column of Metal Organic Resin-Alginic Acid Composite. *Chem. Sci.* 2016, 7 (3), 2427–2436.
- (53) Vaddi, D. R.; Gurugubelli, T. R.; Koutavarapu, R.; Lee, D.-Y.; Shim, J. Bio-Stimulated Adsorption of Cr(VI) from Aqueous Solution

- by Groundnut Shell Activated Carbon@Al Embedded Material. Catalysts 2022, 12 (3), 290.
- (54) Manning, B. A.; Kiser, J. R.; Kwon, H.; Kanel, S. R. Spectroscopic Investigation of Cr(III)- and Cr(VI)-Treated Nanoscale Zerovalent Iron. *Environ. Sci. Technol.* **2007**, *41* (2), 586–592.
- (55) Handbook of X-Ray Photoelectron Spectroscopy: A Reference Book of Standard Spectra for Identification and Interpretation of XPS Data; Moulder, J. F., Stickle, W. F., Sobol, P. E., Bomben, K. D., Chastain, J., King, R. C., Jr., Eds.; Physical Electronics, Incorporation: Eden Prairie, MN, 1995.
- (56) Islam, S. M.; Im, J.; Freeman, A. J.; Kanatzidis, M. G. Ba<sub>2</sub>HgS<sub>5</sub>-a Molecular Trisulfide Salt with Dumbbell-like (HgS<sub>2</sub>)<sup>2-</sup> Ions. *Inorg. Chem.* **2014**, *53* (9), 4698–4704.
- (57) Ma, S.; Huang, L.; Ma, L.; Shim, Y.; Islam, S. M.; Wang, P.; Zhao, L.-D.; Wang, S.; Sun, G.; Yang, X.; Kanatzidis, M. G. Efficient Uranium Capture by Polysulfide/Layered Double Hydroxide Composites. J. Am. Chem. Soc. 2015, 137 (10), 3670–3677.
- (58) Islam, S. M.; Vanishri, S.; Li, H.; Stoumpos, C. C.; Peters, J. A.; Sebastian, M.; Liu, Z.; Wang, S.; Haynes, A. S.; Im, J.; Freeman, A. J.; Wessels, B.; Kanatzidis, M. G. Cs<sub>2</sub>Hg<sub>3</sub>S<sub>4</sub>: A Low-Dimensional Direct Bandgap Semiconductor. *Chem. Mater.* **2015**, *27* (1), 370–378.
- (59) Yuan, M.; Yao, H.; Xie, L.; Liu, X.; Wang, H.; Islam, S. M.; Shi, K.; Yu, Z.; Sun, G.; Li, H.; Ma, S.; Kanatzidis, M. G. Polypyrrole-Mo<sub>3</sub>S<sub>13</sub>: An Efficient Sorbent for the Capture of Hg<sup>2+</sup> and Highly Selective Extraction of Ag<sup>+</sup> over Cu<sup>2+</sup>. *J. Am. Chem. Soc.* **2020**, *142* (3), 1574–1583.
- (60) Xie, L.; Yu, Z.; Islam, S. M.; Shi, K.; Cheng, Y.; Yuan, M.; Zhao, J.; Sun, G.; Li, H.; Ma, S.; Kanatzidis, M. G. Remarkable Acid Stability of Polypyrrole-MoS<sub>4</sub>: A Highly Selective and Efficient Scavenger of Heavy Metals Over a Wide pH Range. *Adv. Funct. Mater.* **2018**, 28 (20), 1800502.
- (61) Huang, W.; Jiao, J.; Ru, M.; Bai, Z.; Yuan, H.; Bao, Z.; Liang, Z. Localization and Speciation of Chromium in Coptis Chinensis Franch. Using Synchrotron Radiation X-Ray Technology and Laser Ablation ICP-MS. Sci. Rep. 2018, 8 (1), 8603.
- (62) Werner, M.; Nico, P.; Guo, B.; Kennedy, I.; Anastasio, C. Laboratory Study of Simulated Atmospheric Transformations of Chromium in Ultrafine Combustion Aerosol Particles. *Aerosol Sci. Technol.* **2006**, *40* (7), 545–556.
- (63) Pinakidou, F.; Kaprara, E.; Katsikini, M.; Paloura, E. C.; Simeonidis, K.; Mitrakas, M. Sn(II) Oxy-Hydroxides as Potential Adsorbents for Cr(VI)-Uptake from Drinking Water: An X-Ray Absorption Study. *Sci. Total Environ.* **2016**, 551–552, 246–253.
- (64) Farges, F. Chromium Speciation in Oxide-Type Compounds: Application to Minerals, Gems, Aqueous Solutions and Silicate Glasses. *Phys. Chem. Minerals* **2009**, *36* (8), 463–481.
- (65) George, S. J.; Drury, O. B.; Fu, J.; Friedrich, S.; Doonan, C. J.; George, G. N.; White, J. M.; Young, C. G.; Cramer, S. P. Molybdenum X-Ray Absorption Edges from 200 20,000 EV, The Benefits of Soft X-Ray Spectroscopy for Chemical Speciation. *J. Inorg. Biochem.* 2009, 103 (2), 157–167.